V European Conference on Computational Fluid Dynamics
ECCOMAS CFD 2010
J. C. F. Pereira and A. Sequeira (Eds)
Lisbon, Portugal,14-17 June 2010

REGULARIZATION MODELING OF WALL-BOUNDED TURBULENT FLOWS

F.Xavier Trias[†,⋆], Andrey Gorobets[†], Roel Verstappen[⋆], Assensi Oliva[†]

[†] Technical University of Catalonia, Centre Tecnològic de Transferència de Calor
ETSEIAT, C/Colom 11, 08222 Terrassa, Spain, e-mail: cttc@cttc.upc.edu

[⋆] Institute of Mathematics and Computing Science, University of Groningen, P.O.Box 407
9700 AK Groningen, The Netherlands, e-mail: r.w.c.p.verstappen@math.rug.nl

Key words: Regularization modeling, LES, turbulence, differentially heated cavity

Abstract.

Since direct numerical simulations cannot be computed at high Reynolds numbers, a dynamically less complex formulation is sought. In the quest for such a formulation, we consider regularizations of the convective term that preserve the symmetry and conservation properties exactly. This requirement yielded a novel class of regularizations (Computers & Fluids 37 (2008) 887) that restrain the convective production of smaller and smaller scales of motion in an unconditionally stable manner, meaning that the velocity cannot blow up in the energy-norm (in 2D also: enstrophy-norm). The numerical algorithm used to solve the governing equations must preserve the symmetry and conservation properties too. To do so, one of the most critical issues is the discrete filtering. The method requires a list of properties that, in general, are not preserved by classical filters for LES unless they are imposed a posteriori. In the present paper, we propose a novel class of discrete filters that preserves such properties per se. They are based on polynomial functions of the discrete diffusive operator, $\tilde{D}$, with the general form $F = I + \sum_{m=1}^{M} d_m \tilde{D}^m$. Then, the coefficients, d_m, follow from the requirement that, at the smallest grid scale k_c, the amount by which the interactions between the wavevector-triples $(k_c, k_c - q, q)$ are damped must become virtually independent of the q-th Fourier-mode. This allows an optimal control of the subtle balance between convection and diffusion at the smallest grid scale to stop the vortex-stretching. Finally, the proposed method is tested for an air-filled differentially heated cavity of height aspect ratio 4.

1 INTRODUCTION

The incompressible Navier-Stokes (NS) equations form an excellent mathematical model for turbulent flows. In primitive variables the equations are

$$\partial_t u + \mathcal{C}(u,u) = \frac{1}{Re}\Delta u - \nabla p\,; \qquad \nabla \cdot u = 0 \tag{1}$$

where u denotes the velocity field, p represents the pressure, Re is the Reynolds number and the non-linear, convective term is defined by $\mathcal{C}(u,v) = (u \cdot \nabla)\, v$.

Preserving the (skew-)symmetries of the continuous differential operators when discretizing them has been shown to be a very suitable approach for direct numerical simulation (DNS) (see[1], for instance). Doing so, certain fundamental properties such as the inviscid invariants - kinetic energy, enstrophy (in 2D) and helicity (in 3D) - are exactly preserved in a discrete sense. However, direct simulations at high Reynolds numbers are not feasible because the convective term produces far too many relevant scales of motion. Therefore, a dynamically less complex mathematical formulation is needed. In the quest for such a formulation, we consider regularizations[2,3] (smooth approximations) of the nonlinearity. The first outstanding approach in this direction goes back to Leray[4]; the Navier-Stokes-α model also forms an example of regularization modeling (see[3], for instance). The regularization methods basically alter the convective terms to reduce the production of small scales of motion. In doing so, we proposed to preserve the symmetry and conservation properties of the convective terms exactly[5]. This requirement yielded a family of *symmetry-preserving regularization* models: a novel class of regularizations that restrains the convective production of smaller and smaller scales of motion in an unconditionally stable manner, meaning that the velocity cannot blow up in the energy-norm (in 2D also: enstrophy-norm). The numerical algorithm used to solve the governing equations preserves the conservation properties too[1] and is therefore well-suited to test the proposed simulation model. The regularization makes use of a normalized self-adjoint filter. In the initial tests[5,6], the performance of the method was tested keeping the ratio filter length/grid width constant. Thus, this parameter had to be prescribed in advance and therefore a convergence analysis was needed. Later, to circumvent this, a parameter-free approach was proposed[7]. To do so, we proposed to determine the regularization parameter (the local filter length) dynamically from the requirement that the vortex-stretching must be stopped at the scale set by the grid. However, in this way, some of the basic properties of the filter (*i.e.*, symmetry, normalization, incompressibility ...) are lost. Therefore, they need to be restored by explicitly forcing them. However, such *a posteriori* modifications are artifacts that may change the dynamics of the system significantly.

In this context, here we propose a family of discrete linear filters that preserve several fundamental properties by construction. To do so, polynomial functions of the discrete diffusive operator are considered. In this way, a list of properties are automatically satisfied *per se*: (i) the filter is exactly symmetric and normalized, (ii) the diffusive nature of

the filter implies that any non-physical transport between scales is introduced and (iii) a filtered divergence-free vector remains 'almost' incompressible. Moreover, since they are only based on the diffusive operator their implementation, even for unstructured formulations, becomes straightforward. Then, the exact coefficients follow from the requirement that the damping of all triadic interactions at the smallest scale must become virtually independent of the interacting wavevectors. The latter is a crucial property to control the subtle balance between convection and diffusion in order to stop the vortex-stretching mechanism. Here, the performance of the proposed method is tested for an air-filled differentially heated with height aspect ratio 4.

2 RESTRAINING THE PRODUCTION OF SMALL SCALES: $\mathcal{C}_n$-REGULARIZATION

2.1 Regularization modeling

At high Re-numbers, the velocity field cannot be computed numerically from the NS equations (1), because the solution possesses far too many scales of motion. The computationally almost numberless small scales result from the nonlinear, convective term $\mathcal{C}(u,u)$ that allow the transfer of energy from scales as large as the flow domain to the smallest scales that can survive viscous dissipation. In the quest for a dynamically less complex mathematical formulation, we consider smooth approximations (regularizations) of the nonlinearity,

$$\partial_t u_\epsilon + \widetilde{\mathcal{C}}(u_\epsilon, u_\epsilon) = \frac{1}{Re}\Delta u_\epsilon - \nabla p_\epsilon\,; \qquad \nabla \cdot u_\epsilon = 0 \tag{2}$$

where the variable names are changed from u and p to u_ϵ and p_ϵ, respectively, to stress that the solution of (2) differs from that of the NS equations.

The regularized system (2) should be more amenable to be solved numerically (that is, the regularization should limit the production of small scales of motion), while the leading modes of u_ϵ have to approximate the corresponding modes of the solution u of equations (1). The regularized system (2) may also be seen in relation to large-eddy simulation (LES). In LES, equations (1) are filtered spatially, and the resulting nonlinear terms involving residual velocities are modeled in terms of the filtered velocity

$$\partial_t \overline{u}_\epsilon + \mathcal{C}(\overline{u}_\epsilon, \overline{u}_\epsilon) = \frac{1}{Re}\Delta \overline{u}_\epsilon - \nabla p_\epsilon + \mathcal{M}(\overline{u}_\epsilon), \tag{3}$$

where the model terms are approximately given by $\mathcal{M}(\overline{u}_\epsilon) \approx \mathcal{C}(\overline{u}_\epsilon, \overline{u}_\epsilon) - \overline{\mathcal{C}(u_\epsilon, u_\epsilon)}$. The regularization described by equations (2) falls in this concept if

$$\overline{\widetilde{\mathcal{C}}(u_\epsilon, u_\epsilon)} = \mathcal{C}(\overline{u}_\epsilon, \overline{u}_\epsilon) - \mathcal{M}(\overline{u}_\epsilon). \tag{4}$$

Indeed under this condition, equations (2) are equivalent to (3): we can filter (2) first and thereafter compare the filtered version of (2) term-by-term with (3) to identify the

closure model $\mathcal{M}(\overline{u}_\epsilon)$. Finally, it may be noted that equation (4) relates the regularization $\widetilde{\mathcal{C}}(u_\epsilon, u_\epsilon)$ one-to-one to the closure model $\mathcal{M}$ for any invertible filter.

2.2 Symmetry-preserving regularization models

The regularization method basically alters the nonlinearity to restrain the production of small scales of motion, (see *e.g.*[3]). In doing so, one can preserve certain fundamental properties of the convective operator $\mathcal{C}$ in equations (1) exactly. We propose to preserve the symmetry properties that form the basis for the conservation of energy, enstrophy (in 2D) and helicity, *i.e.*

$$(\mathcal{C}(u,v),w) = -(v,\mathcal{C}(u,w)), \tag{5}$$
$$(\mathcal{C}(u,v),\Delta v) = (u,\mathcal{C}(\Delta v,v)), \tag{6}$$

where the skew-symmetry with respect to v and w of the trilinear form $(\mathcal{C}(u,v),w)$ ensures the conservation of energy and helicity. Additionally, the identity (6) must be satisfied to conserve enstrophy in 2D. Therefore, we aim to regularize the convective operator $\mathcal{C}$ in such a manner that the underlying symmetries (given by equations (5) and (6)) are preserved. In other words, we require that the approximation $\widetilde{\mathcal{C}}$ of $\mathcal{C}$ satisfies $(\widetilde{\mathcal{C}}(u,v),w) = -(v,\widetilde{\mathcal{C}}(u,w))$, and in 2D, $(\widetilde{\mathcal{C}}(u,v),\Delta v) = (u,\widetilde{\mathcal{C}}(\Delta v,v))$. This criterion yields the following class of regularizations proposed in[5],

$$\mathcal{C}_2(u,v) = \overline{\mathcal{C}(\overline{u},\overline{v})} \tag{7a}$$
$$\mathcal{C}_4(u,v) = \mathcal{C}(\overline{u},\overline{v}) + \overline{\mathcal{C}(\overline{u},v')} + \overline{\mathcal{C}(u',\overline{v})} \tag{7b}$$
$$\mathcal{C}_6(u,v) = \mathcal{C}(\overline{u},\overline{v}) + \mathcal{C}(\overline{u},v') + \mathcal{C}(u',\overline{v}) + \overline{\mathcal{C}(u',v')}, \tag{7c}$$

where a prime indicates the residual of the filter, *e.g.* $u' = u - \overline{u}$, which can be explicitly evaluated, and $\overline{(\cdot)}$ represents a normalized self-adjoint linear filter with filter length ϵ. The difference between $\mathcal{C}_n(u,u)$ and $\mathcal{C}(u,u)$ is of the order ϵ^n (where $n = 2,4,6$) for symmetric filters with filter length ϵ. Note that for a generic, symmetric filter: $u' = \mathcal{O}(\epsilon^2)u$ (see e.g.[8]).

The approximations $\mathcal{C}_n(u_\epsilon, u_\epsilon)$ are stable by construction, meaning that convective terms do not contribute to the evolution of $|u_\epsilon|^2$; hence, the evolution of $|u_\epsilon|^2$ is governed by a dissipative process. Therefore, replacing the convective term in the NS equations by the $\mathcal{O}(\epsilon^n)$-accurate smooth approximation $\mathcal{C}_n(u_\epsilon, u_\epsilon)$ the partial differential equations to be solved result in

$$\partial_t u_\epsilon + \mathcal{C}_n(u_\epsilon, u_\epsilon) = \frac{1}{Re}\Delta u_\epsilon - \nabla p_\epsilon\,; \qquad \nabla\cdot u_\epsilon = 0 \tag{8}$$

For further details about the symmetry-preserving regularization modeling the reader is referred to[5].

2.3 Triadic interactions

To study the interscale interactions in more detail, we continue in the spectral space. The spectral representation of the convective term in the NS equations is given by

$$\mathcal{C}(u,v)_k = i\Pi(k)\sum_{p+q=k}\hat{u}_p q \hat{v}_q, \tag{9}$$

where $\Pi(k) = I - kk^T/|k|^2$ denotes the projector onto divergence-free velocity fields in the spectral space. Taking the Fourier transform of (7a)-(7c), we obtain the evolution of each Fourier-mode $\hat{u}_k(t)$ of $u_\epsilon(t)$ for the $\mathcal{C}_n$ approximation[1]

$$\left(\frac{d}{dt}+\frac{1}{Re}|k|^2\right)\hat{u}_k + i\Pi(k)\sum_{p+q=k} f_n\left(\hat{g}_k,\hat{g}_p,\hat{g}_q\right)\hat{u}_p q\hat{v}_q = F_k, \tag{10}$$

where $\hat{g}_k$ denotes the k-th Fourier-mode of the kernel of the convolution filter, *i.e.*, $\overline{\hat{u}}_k = \hat{g}_k\hat{u}_k$. The mode $\hat{u}_k$ interacts only with those modes whose wavevectors p and q form a triangle with the vector k. Thus, compared with (9), every triad interaction is multiplied by

$$\begin{aligned}
f_2\left(\hat{g}_k,\hat{g}_p,\hat{g}_q\right) &= \hat{g}_k\hat{g}_p\hat{g}_q, && \text{(11a)}\\
f_4\left(\hat{g}_k,\hat{g}_p,\hat{g}_q\right) &= \hat{g}_k\hat{g}_p+\hat{g}_k\hat{g}_q+\hat{g}_p\hat{g}_q-2\hat{g}_k\hat{g}_p\hat{g}_q, && \text{(11b)}\\
f_6\left(\hat{g}_k,\hat{g}_p,\hat{g}_q\right) &= 1-\left(1-\hat{g}_k\right)\left(1-\hat{g}_p\right)\left(1-\hat{g}_q\right). && \text{(11c)}
\end{aligned}$$

Moreover, since for a generic, symmetric convolution filter (see[8], for instance), $\hat{g}_k = 1-\alpha^2|k|^2+\mathcal{O}(\alpha^4)$ with $\alpha^2=\epsilon^2/24$, the damping functions f_n can be approximated by

$$\begin{aligned}
f_2 &\approx 1-\alpha^2\left(|k|^2+|p|^2+|q|^2\right), && \text{(12a)}\\
f_4 &\approx 1-\alpha^4\left(|k|^2|p|^2+|k|^2|q|^2+|p|^2|q|^2\right), && \text{(12b)}\\
f_6 &\approx 1-\alpha^6|k|^2|p|^2|q|^2. && \text{(12c)}
\end{aligned}$$

Therefore, the interactions between large scales of motion ($\epsilon|k|<1$) approximate the NS dynamics up to $\mathcal{O}(\epsilon^n)$, with $n=2,4,6$, respectively. Hence, the triadic interactions between large scales are only slightly altered. All interactions involving longer wavevectors (smaller scales of motion) are reduced. The amount by which the interactions between the wavevector-triple (k,p,q) are lessened depends on the length of the legs of the triangle $k=p+q$. In the case $n=4$, for example, all triadic interactions for which at least two legs are (much) longer than $1/\epsilon$ are (strongly) attenuated, whereas interactions for which at least two legs are (much) shorter than $1/\epsilon$ are reduced to a small degree only.

[1] Here, for simplicity, the subindex ϵ is dropped.

2.4 Stopping the vortex-stretching mechanism

In the initial tests, the performance of the $\mathcal{C}_4$ approximations was tested keeping the ratio ϵ/h (filter length to the grid width) constant. Therefore, only one parameter needed to be prescribed in advance. Later, to circumvent this, a parameter-free approach was proposed[7]. To do so, we determine the regularization parameter (the local filter length) dynamically from the requirement that the vortex-stretching must be stopped at the smallest scale set by the grid, $k_c = \pi/h$. Shortly, the idea behind is to modify the convective operator sufficiently to guarantee that the following inequality is hold

$$\frac{\omega_{k_c} \cdot \mathcal{C}_n(\omega, u)_{k_c}}{\omega_{k_c} \cdot \omega_{k_c}} \leq \frac{1}{Re} k_c^2. \tag{13}$$

In this way, vortex-stretching is restrained enough to prevent a local intensification of vorticity. Then, recalling the evolution equation (10) of the k-th Fourier-mode for the $\mathcal{C}_n$-approximation, previous expression becomes

$$\frac{\omega_{k_c} \cdot \left(\sum_{p+q=k_c} f_n\left(\hat{g}_{k_c}, \hat{g}_p, \hat{g}_q\right) \hat{u}_p q \hat{v}_q \right)}{\omega_{k_c} \cdot \omega_{k_c}} \leq \frac{1}{Re} k_c^2. \tag{14}$$

Note that $f_n\left(\hat{g}_{k_c}, \hat{g}_p, \hat{g}_q\right)$ depends on the filter length ϵ and, in general, on the wavevectors p and $q = k_c - p$. This is an undesirable property because makes very difficult to control the damping effect, f_n, because it cannot be taken out of the summation. To avoid this, filters should be constructed from the requirement that the damping effect of all the triadic interactions at the smallest scale must be virtually independent of the interacting pairs, *i.e.*

$$f_n\left(\hat{g}_{k_c}, \hat{g}_p, \hat{g}_q\right) \approx f_n\left(\hat{g}_{k_c}\right). \tag{15}$$

This is a crucial property to control the subtle balance between convection and diffusion in order to stop the vortex-stretching mechanism.

3 MATHEMATICAL BASIS

The symmetry-preserving regularizations (7a)-(7c) yield uniqueness and the expected regularity properties: for all initial velocities in $H = \{u \in \mathrm{L}^2(\Omega), \nabla \cdot u = 0\}$ where the spatial domain is given by $\Omega = (0, 2\pi)^3$ and periodic boundary conditions are enforced, and $\epsilon > 0$, Eq. (8), with $\mathcal{C}_n$ given by (7a)-(7c), has a unique C^∞ solution. This solution is bounded in $L^\infty(0, T; H) \cap L^2(0, T; V)$, where the time $t \in (0, T)$, with $T > 0$ arbitrary, and $V = \{u \in \mathrm{H}^1(\Omega), \nabla \cdot u = 0\}$). One subsequence converges weakly in $L^2(0, T; V)$ to a weak NS-solution as $\epsilon \to 0$. The proof is in fact a copy of Leray's proof in[4]. So as for Leray's model, any filtering in Eqs. (7a)-(7c) is sufficient to guarantee that the energy cascade stops at a certain scale of motion.

Fifty years after Kolmogorov's landmark papers on the cascade-concept[9,10], Foias *et al.*[11] proved Kolmogorov's results in a mathematically rigorous manner. They proved that the solution (existence is assumed) of the NS-equation - on a periodic box in dimension three - actual has a range of scales with wavenumber κ for which the rate at which energy is transferred (from scales $> \kappa$ to those $< \kappa$) is independent of κ. In this range the energy behaves like $\kappa^{-5/3}$. The proofs by Foias *et al.*are also applicable to the regularized system (8), because the regularization preserves symmetry and conservation properties of the nonlinearity. In this way it can be shown that the solution of the regularized system - on a periodic box in dimension three - actual has a range of scales with wavenumber k for which the rate at which energy is transferred (from scales $> k$ to those $< k$) is independent of k[12]. In this so-called inertial subrange the energy behaves like $k^{-5/3}$. Compared to Navier-Stokes, the inertial subrange is shortened yielding a more amenable problem to solve numerically.

4 PLAYING WITH DISCRETE OPERATORS

The regularizations $\mathcal{C}_n$ given by Eqs. (7a)-(7c) are constructed in a way that the symmetry properties (5) and (6) are exactly preserved. Of course, the same should hold for the numerical approximations that are used to discretize them. To do so, the basic ingredients are twofold: (i) the original NS equations must be discretized preserving the symmetries of the continuous differential operators and (ii) a normalized self-adjoint filter.

4.1 Symmetry-preserving discretization of NS equations

Preserving the symmetries of the continuous differential operators when discretizing them has been shown to be a very suitable approach for DNS of incompressible flows[1]. In short, the temporal evolution of the spatially discrete staggered velocity, u_h, is governed by the following finite-volume discretization of Eq.(8)

$$\Omega \frac{du_h}{dt} + C\left(u_h\right) u_h + D u_h - M^T p_h = 0_h, \tag{16}$$

where the discrete incompressibility constraint reads $M u_h = 0_h$. The diffusive matrix, D, is symmetric and positive semi-definite; it represents the integral of the diffusive flux $-\nabla u \cdot n/Re$ through the faces. The diagonal matrix, Ω, describes the sizes of the control volumes and the approximate, convective flux is discretized as in[1]. The resulting convective matrix, $C(u_h)$, is skew-symmetric, *i.e.* $C(u_h) + C^T(u_h) = 0$. In a discrete setting, the skew-symmetry of $C(u_h)$ implies that

$$C\left(u_h\right) v_h \cdot w_h = v_h \cdot C^T\left(u_h\right) w_h = -v_h \cdot C\left(u_h\right) w_h, \tag{17}$$

for any discrete velocity vectors u_h (if $M u_h = 0_h$), v_h and w_h. Note that Eq.(17) is the discrete analogue of Eq.(5). Then, the evolution of the discrete energy, $\|u_h\|^2 = u_h \cdot \Omega u_h$, is governed by

$$\frac{d}{dt}\|u_h\|^2 = -u_h \cdot \left(D + D^T\right) u_h < 0 \tag{18}$$

where the convective and pressure gradient contributions cancels because of Eq.(17) and incompressibility constraint $Mu_h = 0_h$, respectively. Therefore, even for coarse grids, the energy of the resolved scales of motion is convected in a stable manner: that is, the discrete convective operator transports energy from a resolved scale of motion to other resolved scales without dissipating any energy, as it should do from a physical point-of-view. This forms a good starting point for LES-like simulations (see[13], for instance). For a detailed explanation, the reader is referred to[1].

4.2 Discrete filtering

Filtering is usually done by means of an integral operator with a symmetrical convolution kernel. In a discrete setting, this results into a linear operator $\overline{u}_h \approx \tilde{F} u_h$. To constitute a suitable filter for our application, the following basic properties are required:

i) Symmetry, $\Omega F = (\Omega F)^T$

ii) Normalization, *i.e.* constant velocity vector is unaffected, $F1 = 1$

iii) Given an incompressible velocity field u_h, $Mu_h = 0_h$; $\overline{u}_h$ must be also divergence-free.

iv) Low-pass filtering, *i.e.* only high-frequency components must be effectively damped.

v) The damping effect of $f_n\left(\hat{g}_{k_c}, \hat{g}_p, \hat{g}_q\right)$ must be virtually independent of the interacting pair $(p, q = k_c - p)$, that is Eq.(15) need to be satisfied.

The first three properties are required to ensure that all the symmetry and conservation properties hold exactly[5]. However, in general, they are not satisfied by $\tilde{F}$, therefore we need to redefine our linear filter F as follows

$$F = S - diag\left(S1 - 1\right) \qquad \text{with} \qquad 2S = \Omega_s^{-1}\left\{\Omega\tilde{F} + (\Omega\tilde{F})^T\right\}. \tag{19}$$

Then, the linear map $u_h \mapsto u_h$ defined by Eq.(19) possesses the basic properties (i) and (ii). Then, regarding the point (iii), it must be noted that, in general, a incompressible velocity field, u_h ($Mu_h = 0_h$), does not automatically imply that $\overline{u}_h$ ($u'_h = u_h - \overline{u}_h$ also) is also divergence-free. Although no 'real' mass is lost in terms of the u_h field, $M\overline{u}_h \neq 0_h$ and $M\overline{u'}_h \neq 0_h$ have series implications: the skew-symmetry of the convective operator (17) and consequently the conservation properties that follow from it would be lost. For instance, because of this, the convection term would not be a pure redistributor of energy any more; instead, it becomes an active source or sink of kinetic energy and therefore the stability of the method is lost. This question has been addressed before for a Leray-α

model in[14]. One possible solution to this problem could be to project the filtered velocity onto a divergence-free space,

$$\tilde{u}_h = F u_h, \tag{20}$$
$$\overline{u}_h = \tilde{u}_h + \Omega^{-1} M^T q_h \qquad \text{with} \quad M\overline{u}_h = 0_h. \tag{21}$$

However, an additional Poisson equation, $M\Omega^{-1}M^T q_h = M\tilde{u}$, needs to be solved each time-step. A computationally less demanding approach relies on explicitly forcing the diagonal term of the discrete convective operators, $C(u_h)$, to be equal to zero,

$$\left[C(u_h)\right]_{j,j} = 0 \qquad \forall j. \tag{22}$$

In this way, the skew-symmetry of the convective operator (17) is restored irrespective whether the advective velocity is exactly divergence-free. Both approaches have been tested in[7]. Since no significant differences have been observed, in the view of lower costs, the second approach was chosen.

In conclusion, assuming that the property (iv) is also satisfied, meaning that F constitutes a suitable filter for our application. However, modifications proposed in Eq.(19) and (22) are artifacts that may change the dynamics of the system significantly. This problem becomes especially relevant in the near-wall regions where the non-slip boundary conditions may cause significant compressibility effects on the filtered velocity. Finally, regarding the last property (v) it must be satisfied via the adjustment of the convolution kernel of the linear filter. This is addressed in the following section.

5 CONSTRUCTING THE DISCRETE FILTER

As stated above, a list of properties are required to the linear filter, F, to be suitable for our application. With this in mind, here we propose a novel family of discrete linear filters that preserve the required properties (i)-(iv) by construction. Then, the exact form follows from the last requirement (v), *i.e.* the damping effect $f(\hat{g}_{k_c}, \hat{g}_p, \hat{g}_q)$ must be almost independent of the interacting wavevectors, p and $q = k_c - p$.

5.1 Playing with discrete diffusive operator, D

Here, we propose to construct symmetric linear filters with the general form

$$F = I + \sum_{m=1}^{M} d_m \tilde{D}^m \qquad \text{with} \qquad \tilde{D} = \Omega^{-1} D, \tag{23}$$

where the boundary conditions that supplement the NS equations (1) are applied to (23) too. Then, the convolution kernel of the filter results

$$\widehat{G}_k = 1 + \sum_{m=1}^{M} d_m \widehat{D}_k^m, \tag{24}$$

where $\widehat{D}_k$ denotes the transfer function of discrete diffusive operator, $\tilde{D}$. In this way, all the above-mentioned basic properties (i)-(iii) are automatically satisfied. Shortly, properties (i) and (ii) follow from the symmetry $D = D^T$ and the fact that the unity vector lies on the kernel of D, *i.e.* $D1 = 0$ (see[1] for details). Recalling that $\Delta u = \nabla(\nabla \cdot u) - \nabla \times (\nabla \times u)$, it follows that $\nabla \cdot \Delta u = 0$ if $\nabla \cdot u = 0$ and therefore the property (iii) is also satisfied. In a discrete sense, the latter holds only approximately. Hence, the modification given by (22) is still required.

Furthermore, since they are only based on D and no additional operator is needed, the method is: (i) easy-to-implement, (ii) boundary conditions are already prescribed in the definition of D, (iii) the diffusive nature of the filter implies that any non-physical transport between scales is introduced and (iv) from a parallel point-of-view the construction of filters with large stencils ($M > 1$) is straightforward. Then, hereafter the only thing that remains is to determine the values of the coefficients, d_m, from the requirement that properties (iv) and (v) must be also satisfied. Therefore the influence of the choice of the filter $\widehat{G}_k$ on the so-called bandwidth of f_n has been further analyzed. We restrict ourselves to the $\mathcal{C}_4$ approximation. Here, the analysis will be restricted to the case of 1D filters, without the loss of generality.

5.2 Starting point: 3-point filter

When considering a discrete 3-point symmetric filter in physical space, the associated transfer function is given by $\hat{g}_k = c_0 + 2c_1 cos(kh)$ where h is the grid width. Therefore, the transfer function of the classical 3-point diffusive operator reads

$$\widehat{D}_k = cos(kh) - 1. \tag{25}$$

To simplify the analysis, hereafter we consider $h = 1$. Then, the 3-point filter ($M = 1$) becomes $\widehat{G}_k = (1 - d_1) + d_1 cos(k)$ where the d_1 is given by

$$d_1 = \frac{1}{2} - \frac{\widehat{G}_\pi}{2}. \tag{26}$$

Note that for $h = 1$ the smallest scale is π (see Figure 1, left). Since for $\mathcal{C}_4$, $f(\widehat{G}_\pi, \widehat{G}_p, \widehat{G}_q) = \widehat{G}_\pi(\widehat{G}_p + \widehat{G}_q) + \widehat{G}_p\widehat{G}_q(1 - 2\widehat{G}_\pi)$ and $p = \pi - q$ (see Eq. 11b), the damping function f_3 for the 3-point filter is bounded by $f_4^{3p}(\widehat{G}_\pi, 0)$ and $f_4^{3p}(\widehat{G}_\pi, \pi/2)$

$$f_4^{3p}(\widehat{G}_\pi, 0) = -\widehat{G}_\pi^2 + 2\widehat{G}_\pi, \tag{27}$$

$$f_4^{3p}(\widehat{G}_\pi, \pi/2) = -\frac{1}{2}\widehat{G}_\pi^3 + \frac{1}{4}\widehat{G}_\pi^2 + \widehat{G}_\pi + \frac{1}{4}. \tag{28}$$

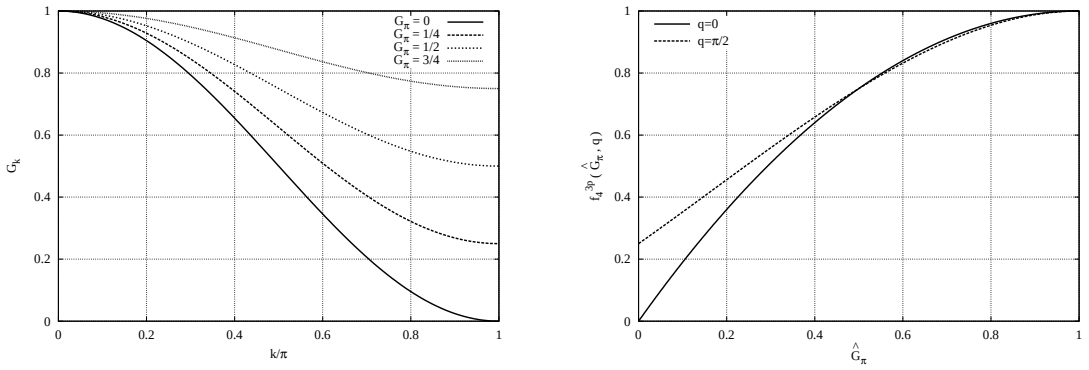

Figure 1: Left: transfer function, $\widehat{G}_k$, for the discrete 3-point filter. Right: bandwidth for $f_4^{3p}(\widehat{G}_\pi, q)$ for the discrete 3-point filter.

Figure 1 (right) shows the bandwidth of $f_4^{3p}(\widehat{G}_\pi, q)$ for $0 \leq \widehat{G}_\pi \leq 1$. For $1/2 \leq \widehat{G}_\pi \leq 1$ it is small and therefore for these values of $\widehat{G}_\pi$, f_4^{3p} can be taken out of the summation (14). However, for $\widehat{G}_\pi \leq 1/2$, the bandwidth of f_4^{3p} increases, and the 3-point filter is no longer satisfactory for taking outside the summation (14).

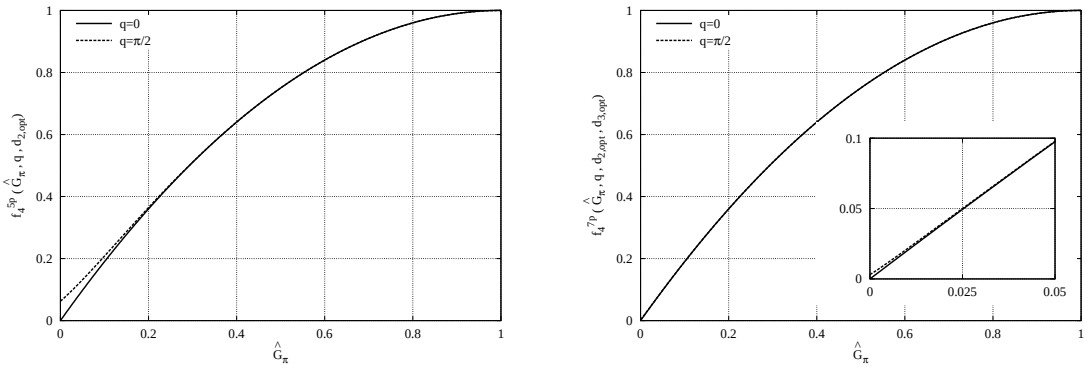

Figure 2: Bandwidth for $f_4^{5p}(\widehat{G}_\pi, q, d_{2,opt})$ (top) and $f_4^{7p}(\widehat{G}_\pi, q, d_{2,opt})$ (bottom) for the discrete 5-point and 7-point filter, respectively.

5.3 Minimizing the bandwidth of $f_4(\widehat{G}_\pi, q)$

Since for the 3-point filter, the coefficient d_1 is given by the condition (26), the bandwidth is fixed. However, additional degrees of freedom, *i.e.* d_2, d_3 ..., may be used to minimize the bandwidth of f_4. This criterion yields the following expressions for a 5- and 7-point discrete filters. The resulting expression for the 5-point filter ($M = 2$) is given by

$$d_{1,opt} = -\frac{\widehat{G}_\pi - 1}{2\widehat{G}_\pi + 1} \qquad d_{2,opt} = \frac{2\widehat{G}_\pi^2 - 3\widehat{G}_\pi + 1}{4\left(2\widehat{G}_\pi + 1\right)}. \tag{29}$$

Then, taking $d_2 = d_{2,opt}$ and $d_1 = d_{1,opt}$, f_4^{5p} is again bounded by $q = 0$ and $q = \pi/2$. Figure 2 (top) shows the bandwidth of $f_4^{5p}(\widehat{G}_\pi, q, d_{2,opt})$. However, the bandwidth of f_4^{5p} for small values of $\widehat{G}_\pi$ may not be small enough. To solve this, an additional degree of freedom is required. Then, the following 7-point filter ($M = 3$) follows

$$\left.\begin{aligned} d_{3,opt} &= \frac{4}{27}\left(\frac{E(\widehat{G}_\pi)}{C(\widehat{G}_\pi)} + \frac{D(\widehat{G}_\pi)}{E(\widehat{G}_\pi)} - \frac{7}{2}\right)\left(\widehat{G}_\pi - 1\right) \\ d_{2,opt} &= 3d_{3,opt} + \frac{1}{2}\sqrt{-2d_{3,opt}^2 - 4d_{3,opt}\widehat{G}_\pi + 4d_{3,opt}} \\ d_{1,opt} &= \frac{1}{2}\left(1 + 4d_{2,opt} - 8d_{3,opt} - \widehat{G}_\pi\right) \end{aligned}\right\} \quad \text{if } 0 \le \widehat{G}_\pi < 1/2 \quad (30)$$

$$d_{1,opt} = -\frac{\widehat{G}_\pi - 1}{2\widehat{G}_\pi + 1} \qquad d_{2,opt} = \frac{2\widehat{G}_\pi^2 - 3\widehat{G}_\pi + 1}{4\left(2\widehat{G}_\pi + 1\right)} \qquad \text{if } 1/2 \le \widehat{G}_\pi \le 1 \quad (31)$$

where $C(\widehat{G}_\pi) = 4\widehat{G}_\pi^2 - 4\widehat{G}_\pi + 1$, $D(\widehat{G}_\pi) = 4\widehat{G}_\pi^2 - 196\widehat{G}_\pi + 1$ and $E(\widehat{G}_\pi) = (C^2(\widehat{G}_\pi)(A(\widehat{G}_\pi) + 12\sqrt{6}\sqrt{\widehat{G}_\pi B(\widehat{G}_\pi)/C(\widehat{G}_\pi)}))^{1/3}$ with $A(\widehat{G}_\pi) = 4\widehat{G}_\pi^2 + 1004\widehat{G}_\pi + 1$ and $B(\widehat{G}_\pi) = 48\widehat{G}_\pi^4 + 4096\widehat{G}_\pi^3 + 4072\widehat{G}_\pi^2 + 1024\widehat{G}_\pi + 3$. Note that for $\widehat{G}_\pi \le 1/2$ it becomes the 5-point filter given by (29) with a smooth transition from f_4^{5p} to f_4^{7p} at $\widehat{G}_\pi = 1/2$. Figure 2 (bottom) shows the bandwidth of $f_4^{7p}(\widehat{G}_\pi, q, d_{2,opt}, d_{3,opt})$. Again, f_4^{7p} is bounded by $q = 0$ and $q = \pi/2$. Now, the bandwidth is small for the whole range $0 \le \widehat{G}_\pi \le 1$ and therefore f_4^{7p} can always be taken out of the summation (14).

6 RESULTS FOR A TURBULENT DHC AT $Ra = 10^{10}$

The performance of the C_4-approximation has been tested for a turbulent differentially heated cavity (DHC) by direct comparison with the DNS reference results[15,16,17]. The coordinate system used here is: x_1 for the periodic direction and x_2 (horizontal) and x_3 (vertical) for the two wall-normal directions (see Figure 3, left). Ra is the Rayleigh number based on the cavity height, $(g\beta\Delta T L_3^3)/(\nu\alpha)$ and $Pr = \nu/\alpha$. To account for the density variations, the Boussinesq approximation is used. Furthermore, if we consider that the cavity is filled with air ($Pr = 0.71$), and that its height aspect ratio, L_3/L_2, is equal to 4, then all that remains is to determine Ra, to fully define the problem. For further details about this configuration the reader is referred to[15,16,17]

Averages over the three statistically invariant transformations (time, x_1-direction and central point symmetry around the center of the cavity) have been carried out. The standard averaging notation, $\langle\cdot\rangle$, is used here. Statistical values have been obtained for a time interval corresponding to ≈ 500 time units of simulation. As initial test, two very coarse meshes (see Table 1) have been used to solve the DHC-problem at $Ra = 10^{10}$.

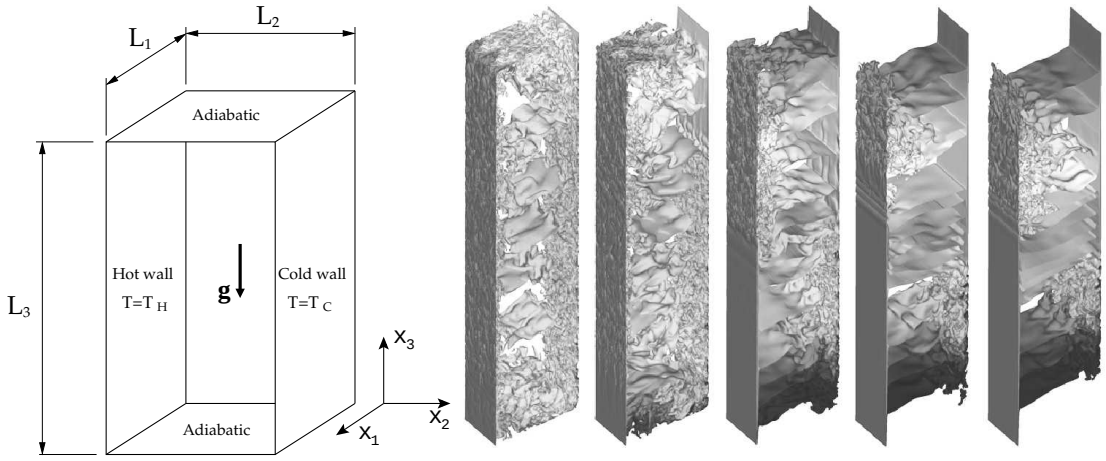

Figure 3: Left: Differentially heated cavity schema. Right: DNS of an air-filled DHC at $Ra = 10^{11}$ and height aspect ratio 4. Several instantaneous temperature fields.

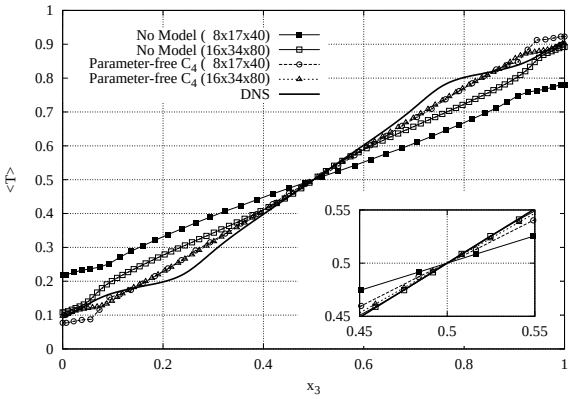

Figure 4: Averaged vertical temperature profile at mid-width.

6.1 Mean fields

The corresponding vertical temperature profile at mid-width is displayed in Figure 4. At first sight we can observe a significant improvement for the smoothed solutions. At the top and bottom areas, where the flow is more turbulent, some discrepancies regarding the reference solution are still observed for both meshes. The fairly good prediction at the cavity core even for the coarsest mesh is especially relevant. Actually, an accurate prediction of thermal stratification of this configuration is a challenge for turbulence modeling. In Figure 5 (left), we can see that without smoothing ($\epsilon = 0$), the thermal stratification is clearly underpredicted, especially for the coarsest mesh.

Let us focus now on the vertical boundary layer. It remains laminar in its upstream part up to the point where the Tollmien-Schlichting waves traveling downstream grow up enough to disrupt the boundary layer (see Figure 3, right). Its high sensitivity to external

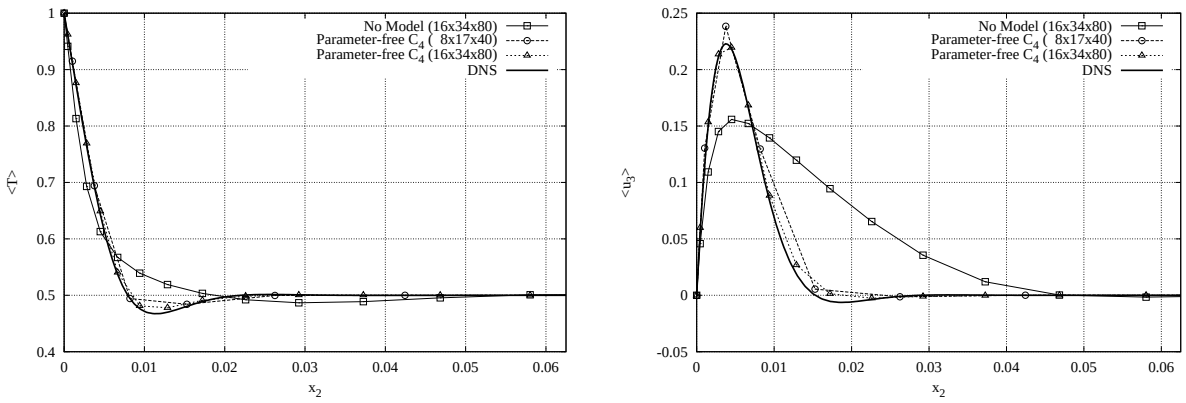

Figure 5: Averaged temperature (left) and vertical velocity (right) profiles at the horizontal mid-height plane.

disturbances makes it difficult to predict. The corresponding temperature and vertical velocity profiles at the cavity mid-height plane, $x_3 = 0.5$, are displayed in Figure 5. As expected, we can observe a strong relation between $\langle T \rangle$ and $\langle u_3 \rangle$: one cannot be predicted well if the other is not. The solutions corresponding to $\epsilon = 0$ (labeled 'No Model') have a the vertical boundary layer that is too thick, whereas with the C_4-smoothing, results for the two coarse meshes agree very well with the DNS reference solution.

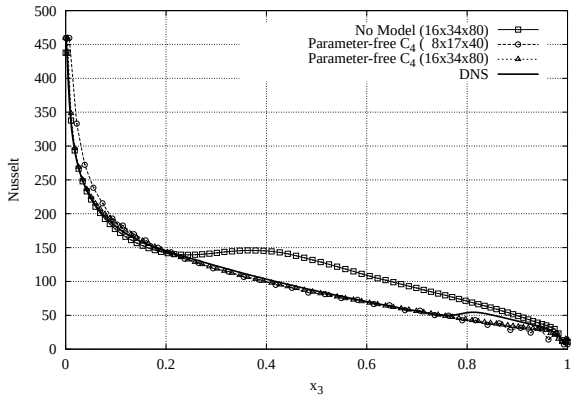

Figure 6: Local Nusselt number distribution.

6.2 Heat transfer

The total Nusselt numbers are shown in Table 1. The reference value $Nu = 101.94$ has been obtained from our DNS simulation[16,17] with $\epsilon = 0$. We see that both C_4 simulations, RM1 and RM2 , predict fairly well the reference value. Moreover, in Figure 7, we observe that the heat transfer is also well captured for all randomly generated meshes whereas the solutions obtained without smoothing ($\epsilon = 0$) are incomparably worse. Results of the

distribution of Nusselt number in the hot wall are shown in Figure 6. A change in the shape is observed at nearly $x_3 = 0.2$ for the non-smoothed results, indicating a much too early transition toward turbulence. In contrast, the C_4 results are able to capture well most of the profile except for the most upstream part where the heat transfer is slightly underpredicted.

	DNS	RM1		RM2	
Mesh	$128\times190\times462$	$16\times34\times80$		$8\times17\times40$	
		No model	C_4	No model	C_4
Nu	101.94	121.93	100.81	128.14	102.17
Nu_{max}	454.86	437.78	451.12	342.02	459.59
Nu_{min}	8.50	10.92	10.18	27.77	7.03

Table 1: The overall, the maximum and the minimum of the averaged Nusselt number.

In Table 1, the maximum and the minimum values of the local Nusselt number are also shown. These two quantities are of interest because they occur in two clearly different parts of the vertical boundary layers. Maximum values occur in the upstream part of the boundary layer where it is still almost laminar whereas minimum values are observed at the most downstream part of the boundary layer where it has become fully turbulent. For both coarse grids, the significant improvements are achieved for the smoothed solutions.

6.3 Grid (in)dependence analysis

A reliable modeling of turbulence at (very) coarse grids is a great challenge. The coarser the grid, more convincing model quality is perceived. However, it might happen that the solution is strongly dependent on meshing parameters and thus some particular combinations could 'accidentally' provide good results. An example of this behavior has been observed in[18] for a turbulent channel flow. In order to elucidate this point, the same DHC problem has been solved on a series of 50 randomly generated meshes: with (N_1, N_2, N_3)-values limited by those given by meshes RM1 and RM2 (see Table 1), *i.e.*, $8 \le N_1 \le 16$, $17 \le N_2 \le 34$, and $40 \le N_3 \le 80$. The concentration parameters are kept equal to those used for the DNS simulation[15]. Note than some of the numerical experiments displayed in Figure 7 correspond to highly skewed grids. Results for the overall Nusselt and the centerline stratification values are displayed in Figure 7 (left). At first sight, we can observe that the C_4 modeling predicts results well irrespective of the meshing whereas very poor and dispersed results are obtained when the model is switched off. The fairly good prediction of the stratification (note the dispersion obtained without model!!) is especially important. Results for the maximum vertical velocity and the wall shear stress scaled at the horizontal mid-height plane, $x_3 = 0.5$, display essentially the same (see Figure 7, right).

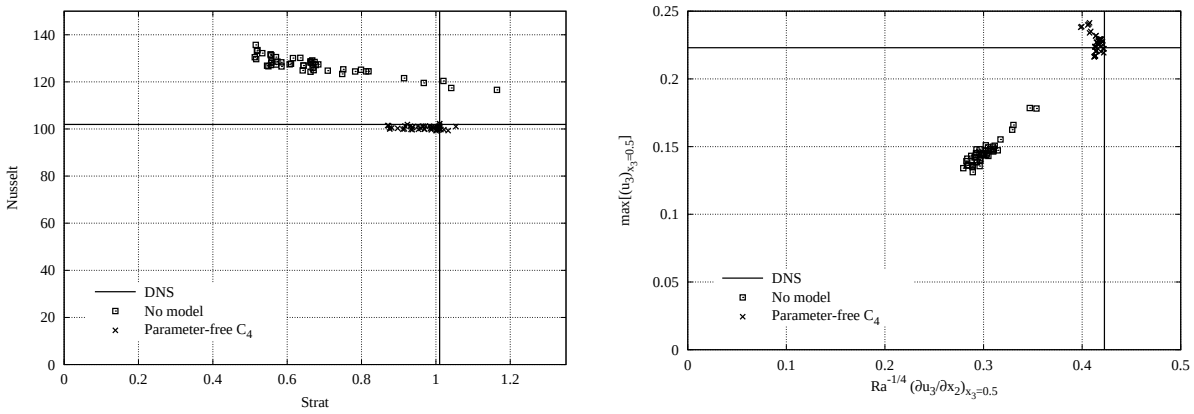

Figure 7: Left: the overall Nusselt number and the centerline stratification. Right: the maximum vertical velocity and the wall shear stress scaled by $Ra^{-1/4}$ at the horizontal mid-height plane. Results have been obtained for 50 randomly generated grids.

7 PERFORMANCE AT HIGHER (AND LOWER) RAYLEIGH NUMBERS

The performance of the C_4-regularization has also been tested at higher (and lower) Ra. This study covers a relatively wide range, $6.4 \times 10^8 \leq Ra \leq 10^{11}$, from weak to fully developed turbulence. Within this range DNS results for five different configurations (at $Ra = 6.4 \times 10^8$, 2×10^9, 10^{10}, 3×10^{10} and 10^{11}, respectively) are available[16,17]. The meshes used to carry out these simulations have been generated keeping the same number of points in the boundary layer as in the coarse mesh RM1 for $Ra = 10^{10}$. In this way, the meshes[2] for $Ra = 3 \times 10^{10}$ and 10^{11} become $10 \times 19 \times 46$ with $\gamma_2 = 2.26$ and $12 \times 26 \times 62$ with $\gamma_2 = 2.28$, respectively.

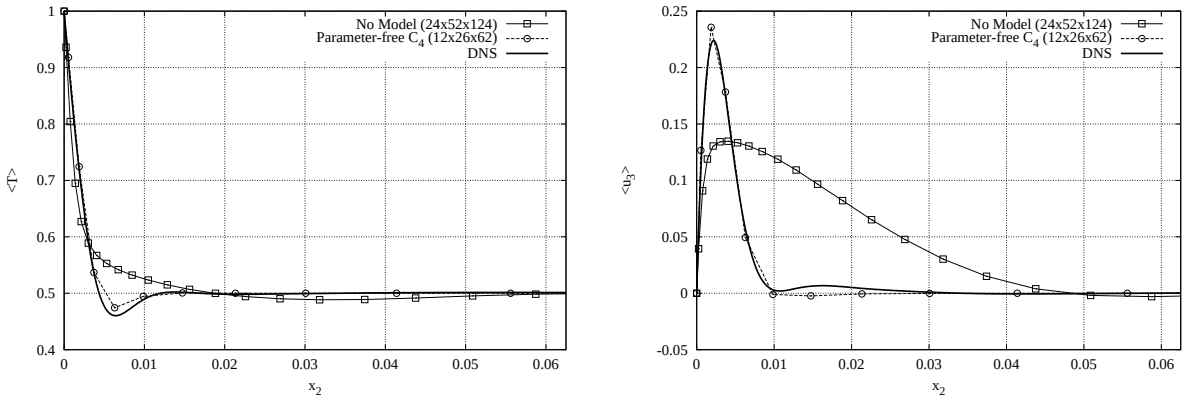

Figure 8: Averaged temperature (left) and vertical velocity (right) profiles at the horizontal mid-height plane at $Ra = 10^{11}$.

[2]Note that the grid stretching near the vertical walls has also been slightly increased with the Ra.

7.1 Boundary layer

For the sake of brevity, in this section we focus only on the highest Ra, *i.e.* 10^{11}. In Figure 8, the temperature and the vertical velocity profiles at the horizontal mid-height plane, $x_3 = 0.5$, are displayed. Again, the C_4 method and non-smoothed results ($\epsilon = 0$) obtained using a mesh that it is twice finer in each direction are compared with DNS data. All plots depict essentially the same: the C_4 method is able to capture well the flow structure of the vertical boundary layer even for the coarsest meshes whereas the results of the non-smoothed simulations differ largely from the reference solution.

7.2 Heat transfer

The heat flux as a function of Rayleigh number is investigated in this section. In the last decades significant efforts, both numerical and experimentally, have been directed at investigating the mechanisms and detailed scaling behavior on turbulent Rayleigh-Bénard (RB) problems. Classical theory predicts that $Nu \sim Ra^{\xi}$ with $\xi = 1/3$. Alternative scaling theories, encouraged by experimental observations, lead to $\xi = 2/7$[19]. Finally, an asymptotic regime, the so-called Kraichnan regime, with $\xi = 1/2$ is presumed to exist at very high Ra. Experimentally, power-law dependencies of heat flux with exponents between $1/4$ and $1/3$ have been measured[20]. Regarding the Kraichnan regime, and despite the great efforts devoted, no clear evidence has been observed yet[21]. On the other hand, there is still controversy whether a simple power-law $Nu \sim Ra^{\xi}$ is adequate[20]. Comparatively, the DHC problem has received much less attention from the scientific community. Nevertheless, both configurations share similar heat transfer scaling[22] and most of the ideas applied to RB configuration can be easily applied to the DHC problem. In[17] we found that $Nu \approx 0.182 Ra^{0.275}$ was the power-law scaling that fitted best our DNS results. Actually, this exponent cannot be considered 'near' $1/3$; rather, it is closer to the $2/7 \approx 0.286$ proposed by alternatives theories of turbulent natural convection flows[19].

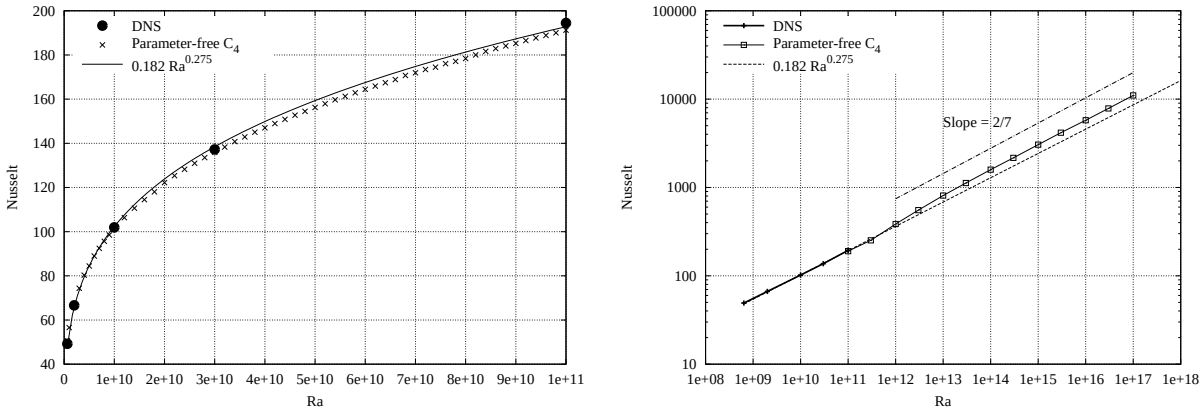

Figure 9: Overall Nusselt number for $6.4 \times 10^8 \leq Ra \leq 10^{11}$ (left) and for Ra up to 10^{17} (right).

7.2.1 Comparison with DNS results

Results for the overall Nusselt number corresponding to 56 simulations within the whole range of Rayleigh numbers studied by DNS, *i.e.*, $6.4 \times 10^8 \leq Ra \leq 10^{11}$, are displayed in Figure 9 (left). At first sight, we observe again a fairly good agreement with the DNS results (solid dots) and the correlation obtained from the DNS data. It must be noted that the Nu-Ra dependence obtained with the C_4 is smooth suggesting again that the proposed model is performing well 'independently' of Ra and meshing parameters that may suddenly change for two consecutive points in the graph.

7.2.2 Nu-number correlation with Ra up to 10^{17}

Since performing computations with the C_4 approximation is rather cheap simulations at very high Ra have also been performed. Following the aforesaid criteria to keep the number of point at the vertical boundary layer constant leads to a $68 \times 142 \times 334$ mesh with $\gamma_2 = 3.48$ for $Ra = 10^{17}$. Of course, for the range $10^{11} < Ra \leq 10^{17}$ there is no DNS (or experimental) data to compare with. Anyhow, it is interesting to see that results displayed in Figure 9 (right) show a good agreement with a 2/7 power-law scaling of Nusselt (Nu increases approximately from 10^2 to 10^4, that is 2 orders of magnitude, when Ra is increased 7 orders, from 10^{10} to 10^{17}). This scaling law, predicted by alternatives theories[19] of turbulent natural convection, has also been experimentally measured for RB configurations[21].

8 CONCLUDING REMARKS

The $\mathcal{C}_4$-regularization of the nonlinear convective term has been considered as a simulation shortcut. The symmetries and conservation properties of the original convective term are exactly preserved. Doing so, the production of smaller and smaller scales of motion is restrained in an unconditionally stable manner. The numerical algorithm to solve the governing equations is also fully-conservative and is therefore well-suited to test the proposed simulation method. Here, a novel family of discrete linear filters have been proposed. They are based on polynomial functions of the discrete Laplacian operator. In this way, all the required properties are automatically satisfied.

An air-filled DHC with height aspect ratio 4 has been used as test case for the $\mathcal{C}_4$-regularization method together with the new family of filters. This is a challenging configuration for turbulence modeling since areas with completely different regimes coexist and interplay. Direct comparison with DNS reference results within a relatively wide range of Rayleigh numbers, $6.4 \times 10^8 \leq Ra \leq 10^{11}$, has shown that the method is able to capture the general pattern of the flow correctly even for very coarse meshes. The robustness of the method has been tested by performing simulations for a series of randomly generated grids. Even for highly skewed grids, all the results obtained with the $\mathcal{C}_4$ method were clustered around the DNS reference solution. Finally, to study the heat

transfer scaling, simulations at higher Ra up to 10^{17} have also been computed. A fairly good agreement with a 2/7 power-law scaling of Nusselt has been measured for the whole range, *i.e.*$10^{11} \leq Ra \leq 10^{17}$. This scaling law, also predicted by alternatives theories of turbulent natural convection, has also been experimentally measured for RB configurations.

We can conclude that these results illustrate the great potential of the $\mathcal{C}_4$ smoothing method as a simulation shortcut. Nevertheless, more simulations for a wide variety of cases and meshes will be necessary to confirm these preliminary conclusions.

ACKNOWLEDGEMENTS

This work has been financially supported by the *Ministerio de Educación y Ciencia*, Spain, (Project: "Development of high performance parallel codes for the optimal design of thermal equipments". Contract/grant number ENE2007-67185) and a postdoctoral fellowship *Beatriu de Pinós* (2006 BP-A 10075) by the *Generalitat de Catalunya*.

Reference DNS results have been performed on the IBM MareNostrum supercomputer at the Barcelona Supercomputing Center. The authors thankfully acknowledge this institution.

References

[1] R. W. C. P. Verstappen, A. E. P. Veldman, Symmetry-Preserving Discretization of Turbulent Flow, Journal of Computational Physics 187 (2003) 343–368.

[2] J. L. Guermond, J. T. Oden, S.Prudhomme, Mathematical perpectives on large eddy simulation models for turbulent flows, Journal of Mathematical Fluid Mechanics 6 (2004) 194–248.

[3] B. J. Geurts, D. D. Holm, Regularization modeling for large-eddy simulation, Physics of Fluids 15 (2003) L13–L16.

[4] J. Leray, Sur le movement d'un liquide visqueaux emplissant l'espace, Acta Mathematica 63 (1934) 193–248.

[5] R. Verstappen, On restraining the production of small scales of motion in a turbulent channel flow, Computers and Fluids 37 (2008) 887–897.

[6] F. X. Trias, M. Soria, A. Oliva, R. W. C. P. Verstappen, Regularization models for the simulation of turbulence in a differentially heated cavity, in: Proceedings of the European Computational Fluid Dynamics Conference (ECCOMAS CFD 2006), Egmond aan Zee, The Netherlands, 2006.

[7] F. X. Trias, R. W. C. P. Verstappen, A. Gorobets, M. Soria, A. Oliva, Parameter-free symmetry-preserving regularization modelling of a turbulent differentially heated cavity, Computers and Fluids (under revision).

[8] D. Carati, G. S. Winckelmans, H. Jeanmart, Exact expansions for filtered-scales modelling with a wide class of LES filters, in: Direct and Large-Eddy Simulation III, Kluwer, 1999, pp. 213–224.

[9] A. Kolmogorov, Dissipation of energy in locally isotropic turbulence, Dokl. Akad. Nauk SSSR 32 (1941) 19–21.

[10] A. Kolmogorov, The local structure of turbulent motion in an incompressible fluid, Dokl. Akad. Nauk SSSR 30 (1941) 299–303.

[11] C. Foias, O. Manley, R. Rosa, R. Temam, Estimates for the energy cascade in three-dimensional turbulent flows, C.R. Acad. Sci. Paris I 333 (2001) 499–504.

[12] R. Verstappen, On the inertial range of symmetry-preserving regularization models for turbulent flow, in: Proc. Appl. Math. Mech., Vol. 7, Wiley, 2007, pp. 1100901–1100902.

[13] K. Mahesh, G. Constantinescu, P. Moin, A numerical method for large-eddy simulation in complex geometries, Journal of Computational Physics 197 (2004) 215–240.

[14] M. van Reeuwijk, H. J. J. Jonker, K. Hanjalić, Incompressibility of the Leray-α model for wall-bounded flows, Physics of Fluids 18 (1) (2006) 018103.

[15] F. X. Trias, M. Soria, A. Oliva, C. D. Pérez-Segarra, Direct numerical simulations of two- and three-dimensional turbulent natural convection flows in a differentially heated cavity of aspect ratio 4, Journal of Fluid Mechanics 586 (2007) 259–293.

[16] F. X. Trias, A. Gorobets, M. Soria, A. Oliva, Direct numerical simulation of a differentially heated cavity of aspect ratio 4 with Ra-number up to 10^{11} - Part I: Numerical methods and time-averaged flow, International Journal of Heat and Mass Transfer 53 (2010) 665–673.

[17] F. X. Trias, A. Gorobets, M. Soria, A. Oliva, Direct numerical simulation of a differentially heated cavity of aspect ratio 4 with Ra-number up to 10^{11} - Part II: Heat transfer and flow dynamics, International Journal of Heat and Mass Transfer 53 (2010) 674–683.

[18] J. Meyers, P. Sagaut, Is plane-channel flow a friendly case for the testing of large-eddy simulation subgrid-scale models?, Physics of Fluids 19 (2007) 048105.

[19] B. Castaing, G. Gunaratne, F. Heslot, L. Kadanoff, A. Libchaber, S. Thomae, X. Wu, S. Zaleski, G. Zanetti, Scaling of hard thermal turbulence in Rayleigh-Bénard convection, Journal of Fluid Mechanics 204 (1) (1989) 1–30.

[20] S. Grossmann, D. Lohse, Scaling in thermal convection: a unifying theory, Journal of Fluid Mechanics 407 (2000) 27–56.

[21] J. Sommeria, The elusive 'ultimate state' of thermal convection, Nature 398 (1999) 294–295.

[22] H. Yu, N. Li, R. E. Ecke, Scaling in laminar natural convection in laterally heated cavities: Is turbulence essential in the classical scaling of heat transfer?, Physical Review E 76 (2007) 026303.